Critical phenomena and noise-induced phase transitions in neuronal networks

K.-E. Lee,[1] M. A. Lopes,[1] J. F. F. Mendes,[1] and A. V. Goltsev[1,2]
[1]*Department of Physics & I3N, University of Aveiro, 3810-193 Aveiro, Portugal*
[2]*Ioffe Physical-Technical Institute, 194021 St. Petersburg, Russia*
(Received 14 April 2013; revised manuscript received 16 October 2013; published 2 January 2014)

We study numerically and analytically first- and second-order phase transitions in neuronal networks stimulated by shot noise (a flow of random spikes bombarding neurons). Using an exactly solvable cortical model of neuronal networks on classical random networks, we find critical phenomena accompanying the transitions and their dependence on the shot noise intensity. We show that a pattern of spontaneous neuronal activity near a critical point of a phase transition is a characteristic property that can be used to identify the bifurcation mechanism of the transition. We demonstrate that bursts and avalanches are precursors of a first-order phase transition, paroxysmal-like spikes of activity precede a second-order phase transition caused by a saddle-node bifurcation, while irregular spindle oscillations represent spontaneous activity near a second-order phase transition caused by a supercritical Hopf bifurcation. Our most interesting result is the observation of the paroxysmal-like spikes. We show that a paroxysmal-like spike is a single nonlinear event that appears instantly from a low background activity with a rapid onset, reaches a large amplitude, and ends up with an abrupt return to lower activity. These spikes are similar to single paroxysmal spikes and sharp waves observed in electroencephalographic (EEG) measurements. Our analysis shows that above the saddle-node bifurcation, sustained network oscillations appear with a large amplitude but a small frequency in contrast to network oscillations near the Hopf bifurcation that have a small amplitude but a large frequency. We discuss an amazing similarity between excitability of the cortical model stimulated by shot noise and excitability of the Morris-Lecar neuron stimulated by an applied current.

DOI: 10.1103/PhysRevE.89.012701 PACS number(s): 87.19.lj, 05.70.Fh, 87.19.lc, 87.19.ln

I. INTRODUCTION

In the brain, interactions among neurons lead to diverse collective phenomena such as, for example, self-organization, phase transitions, brain rhythms, and avalanches [1–3]. Among phase transitions, one can mention a nonequilibrium second-order phase transition observed in human bimanual coordination [4–6]. Brain rhythms, epileptic seizures, and the ultraslow oscillations of BOLD fMRI patterns may also emerge as a result of nonequilibrium second-order phase transitions [7]. Living neural networks stimulated by an electric field undergo a first-order phase transition that can be seen as a jump of neuronal activity at a certain applied voltage [8]. Taking into account the role played by the collective phenomena in brain dynamics, it is very important to understand their nature and mechanisms. It is well known that bifurcations are responsible for the emergence of oscillations in nonlinear dynamic models [9,10], for example, the Hodgkin-Huxley model of a biological neuron [11,12]. In the context of brain rhythms, the Hopf bifurcation was discussed in the framework of mean-field cortical models [7], models of randomly connected integrate-and-fire neurons [13–20], and networks of stochastic spiking neurons [21,22]. However, when studying a phase transition, it is not enough to identify the type of bifurcation. It is also necessary to reveal and study critical phenomena accompanying the transition [23]. In the brain, various patterns of spontaneous activity representing collective phenomena were observed, such as neuronal avalanches [2,24,25], paroxysmal activity [26,27], sharp waves in hippocampus [3,28,29], spindle oscillations [30], and many others. Despite a significant progress, understanding of collective phenomena in the brain and bifurcation mechanisms of phase transitions is elusive.

A neuronal network undergoes a phase transition from one to another state when a control parameter, such as an applied voltage or a flow of spikes bombarding neurons, reaches a critical value. In many cases (for example, for epileptic seizures) [31], it is necessary to foresee that a neuronal network approaches to the critical point. An analysis of patterns and statistics of spontaneous neuronal activity and critical phenomena near the critical point may be a useful method for solving the problem. Nowadays, a comprehensive analysis of the critical phenomena in neuronal networks is far from being complete.

In statistical physics, exactly solved models largely help us to understand phase transitions and critical phenomena [32]. Unfortunately, even simple versions of neuronal networks composed of integrate-and-fire neurons are very complex for an analytical consideration [13–20]. In this paper, we study analytically and numerically an exactly solvable cortical model with stochastic excitatory and inhibitory neurons on complex networks. In the framework of this model, we consider first- and second-order phase transitions stimulated by shot noise (a flow of random spikes bombarding neurons). We also study critical phenomena accompanying the transitions and patterns of spontaneous activity signaling the transitions. First, we study a noise-induced first-order phase transition from low to high neuronal activity. The transition occurs if inhibitory neurons respond faster on stimuli than excitatory neurons. We demonstrate that bursts and avalanches of neuronal activity precede the transition. Second, we study two noise-induced second-order phase transitions that occur if inhibitory neurons respond slower on stimuli than excitatory neurons. The transitions represent two scenarios of appearance and disappearance of sustained network oscillations. We show that, when increasing the shot noise intensity, at first, sustained network oscillations appear due to a saddle-node bifurcation and then, at a higher shot noise intensity, the oscillations disappear due to a supercritical Hopf bifurcation.

We study patterns of spontaneous neuronal activity near the bifurcations. We show that sharp paroxysmal-like spikes of activity precede the second-order phase transition caused by the saddle-node bifurcation. Above the Hopf bifurcation, spontaneous activity appears in a form of irregular spindles formed by damped oscillations. We also study analytically and numerically sustained network oscillations near the critical points of the bifurcations. Furthermore, we analyze the power spectral density (PSD) of spontaneous neuronal activity and its dependence on the noise intensity. We show that the PSD depends strongly on the bifurcation mechanism and the closeness to the critical point. We compare our results with experimental data and previous theoretical investigations. Finally, we discuss an amazing similarity between excitability of the considered cortical model stimulated by shot noise and excitability of the Morris-Lecar neuron [33] stimulated by an applied current.

II. MODEL

We study a cortical model composed of N_e excitatory and N_i inhibitory neurons. $N_e + N_i \equiv N$ is the network size, $g_{e(i)} \equiv N_{e(i)}/N$ is the fraction of excitatory (inhibitory) neurons. Neurons are randomly connected with probability c/N by directed edges and form a random directed graph with Poisson degree distribution and the mean in and out degree c.

The network is locally treelike and has the small-world properties [34–36] similar to those found in brain networks [37]. Our model also takes into account noise playing an important role in the brain dynamics [38–41]. We assume that neurons are bombarded by random spikes represented by Dirac delta functions

$$I(t) = \sum_i q\delta(t - t_i), \tag{1}$$

where t_i are arrival times of spikes and q is their amplitude. This kind of random input is so-called shot noise. The flow of random spikes bombarding neurons represents a combined effect of synaptic noise (spontaneous release of neurotransmitters), stimuli from other brain areas or sensory stimuli. According to Schottky's result, in the case of the Poisson distribution of interspike intervals, the power spectral density $S(\omega)$ is proportional to the mean frequency ω_{sn} of spikes $S(\omega) = 2q^2\omega_{sn}$. In this paper, we assume that the probability to receive ξ random spikes during the integration time τ is Gaussian

$$G(\xi) = G_0 \exp[-(\xi - \langle n\rangle)^2/2\sigma^2], \tag{2}$$

where σ^2 is the variance, $\langle n\rangle = \omega_{sn}\tau$ is the mean number of spikes arriving during the time interval τ, and G_0 is the normalization constant $\sum_{\xi=0}^{\infty} G(\xi) = 1$. We use $\langle n\rangle$ as the control parameter characterizing the shot noise intensity.

Neurons also receive deltalike spikes from active neighbors. The spikes mediate interaction among neurons. We assume that efficacies of synaptic connections with excitatory and inhibitory neurons are uniform and equal to J_e ($J_e > 0$) and J_i ($J_i < 0$), respectively. The total input $I(t)$ includes spikes from shot noise and excitatory and inhibitory presynaptic neurons. We define the input V_n to a neuron with index n, $n = 1,2,\ldots,N$, as the integral of $I(t)$ over the time interval $[t - \tau,t]$. It gives

$$V_n(t) = \xi q + kJ_e + lJ_i, \tag{3}$$

where ξ, k, and l are the numbers of spikes arriving during the time interval $[t - \tau,t]$ from shot noise and active presynaptic excitatory and inhibitory neurons, respectively. The numbers k and l are random and are determined by activity of presynaptic neurons during the interval $[t - \tau,t]$. The network structure is encoded in the adjacency matrix.

In our model, neurons are tonic and the firing frequency $f(V)$ versus input V is the Heaviside function

$$f(V) = f\Theta(V - V_{th}), \tag{4}$$

where V_{th} is a threshold. The frequency f is the same for both excitatory and inhibitory neurons. If $f\tau \ll 1$ and spike emission times of neurons are uncorrelated, then during the time interval $[t - \tau,t]$, each active presynaptic neuron contributes to $V_n(t)$ either one spike with probability τf or none with probability $1 - \tau f$.

We consider stochastic neurons such as those of [21,22,42,43]. It means that the response of a neuron to an input is a stochastic process. Such a stochastic behavior might be caused by cellular noise and intensive bombardment by random spikes.

Two rules determines dynamics of the cortical model:

(1) If the input $V_n(t)$ to an inactive excitatory (inhibitory) neuron n at time t is at least a certain threshold V_{th}, then this neuron is activated with probability $\mu_e\tau$ ($\mu_i\tau$) and fires spikes.

(2) An active excitatory (inhibitory) neuron n is inactivated with probability $\mu_e\tau$ ($\mu_i\tau$) if $V_n(t) < V_{th}$.

We introduce a dimensionless activation threshold $\Omega \equiv V_{th}/J_e$. Ω is of the order of 15–30 in living neuronal networks [8,44,45] and about 30–400 in the brain. In our model, $1/\mu_e$ and $1/\mu_i$ are of the order of the first-spike latencies of excitatory and inhibitory neurons (from 6 to 100 ms in the cortex [46–49]). We introduce a parameter

$$\alpha \equiv \mu_i/\mu_e. \tag{5}$$

If inhibitory neurons respond faster to stimuli than excitatory neurons, i.e., the response time $T_i = 1/\mu_i$ of an inhibitory neuron is smaller than the response time $T_e = 1/\mu_e$ of an excitatory neuron, then $\alpha = T_e/T_i > 1$. If excitatory neurons respond faster, i.e., $T_e < T_i$, then $\alpha < 1$. In the cortex, α may be both larger and smaller than 1 [46–49].

A. Rate equations

The behavior of the cortical model is described by the fractions $\rho_e(t)$ and $\rho_i(t)$ of active excitatory and inhibitory neurons, respectively, at time t. We will call them "activities." We assume that activities are changed slightly during the integration time τ. Using the rules formulated above and the methods developed in [42,43,50], in particular, the method of generating functions [43], in the limit $N \to \infty$, we find explicit rate equations

$$\begin{aligned}\dot\rho_e(t) &= F_e(t)[1-\rho_e(t)] - \mu_e\rho_e(t) + \mu_e\Psi_e[\rho_e(t),\rho_i(t)],\\ \dot\rho_i(t) &= F_i(t)[1-\rho_i(t)] - \mu_i\rho_i(t) + \mu_i\Psi_i[\rho_e(t),\rho_i(t)],\end{aligned} \tag{6}$$

where $\dot{\rho} \equiv d\rho/dt$. $\Psi_{e(i)}(\rho_e,\rho_i)$ is the probability that, at given activities ρ_e and ρ_i, input to a randomly chosen excitatory (inhibitory) neuron is at least Ω. F_e and F_i represent fields acting on excitatory and inhibitory neurons. Note that the rate equations (6) are similar to the Wilson-Cowan equations [51] and rate equations derived for a stochastic rate model in [21,22]. In the case of the classical random graph, we find

$$\Psi_i(\rho_e,\rho_i) = \Psi_e(\rho_e,\rho_i) \equiv \Psi(\rho_e,\rho_i) = \sum_{k,l,\xi=0}^{\infty} \Theta(kJ_e + lJ_i + \xi q - \Omega J_e) \times G(\xi) P_k(g_e\rho_e\widetilde{c}) P_l(g_i\rho_i\widetilde{c}), \quad (7)$$

where $\widetilde{c} \equiv c\tau f$. $G(\xi)$, $P_k(g_e\rho_e\widetilde{c})$, and $P_l(g_i\rho_i\widetilde{c})$ are the probabilities that, during the time interval τ, a randomly chosen neuron receives ξ random spikes from shot noise, k spikes from excitatory neurons, and l spikes from inhibitory neurons, respectively. Note that the Poisson function $P_k(c) \equiv c^k e^{-c}/k!$ is the probability that a randomly chosen neuron has k presynaptic connections. In the following, we will study analytically and numerically Eqs. (6) and compare with simulations of the cortical model.

Our cortical model based on [42] is similar to the stochastic model of spiking neurons proposed by Benayoun *et al.* [21]. Both models consider networks of stochastic neurons ("input-dependent stochastic switches" by [21]). The difference between the models is in some details about how to describe activation and deactivation processes and external input. Benayoun *et al.* [21] assume that each neuron spikes with a rate dependent on its total synaptic input, while the resulting spiking activity decays at a constant rate independent on the input. In our model, we use a similar activation rule, while spiking activity decays with a certain rate only if the input becomes smaller than a threshold. The rates for activation and decay are different in [21], in contrast to our model where they are the same. Benayoun *et al.* assume that external input to each neuron is fixed in contrast to our model where external input is represented by shot noise. It is not surprising that, despite these differences, these models demonstrate similar dynamics. The advantage of the models with stochastic neurons is that they can be solved explicitly. Benayoun *et al.* [21] and Wallace *et al.* [22] derived explicit rate equations for networks with all-to-all connections while sparse randomly connected networks (classical random networks) were studied numerically.

Methods of complex network theory [50] allowed us to find explicit rate equations for neuronal networks on classical random graphs [43] and scale-free networks [43] and apply the model to study stochastic resonance [52] and the role of synaptic plasticity [53].

B. Algorithm of simulations and parameters

In simulations, we built a directed network, linking neurons with the probability c/N. We divided time into intervals of width $\Delta t = \tau$. At each time step, for each neuron we calculated input Eq. (3) given that each active presynaptic neuron contributes a spike with probability τf. The number of random spikes (shot noise) in this input was generated by the Gaussian process $G(\xi)$. Then, we updated states of neurons, using the rules formulated above. In our paper, we present numerical calculations for parameters $N = 10^5$, $c = 10^3$, $\Omega = 30$, $\tau f = 0.1$, $f = \mu_e$, and $g_i = 0.25$. We analyze dynamics of the cortical model in dependence on only two parameters: the parameter α and the shot noise intensity. The latter parameter is the control parameter. Throughout this paper, we use $1/\mu_e \equiv 1$ as time unit and $J_e \equiv 1$ as input unit. Following [13], we choose $J_i = -3J_e$. We use $q = J_e$ and $\sigma^2 = 10$ for the amplitude and variance of shot noise.

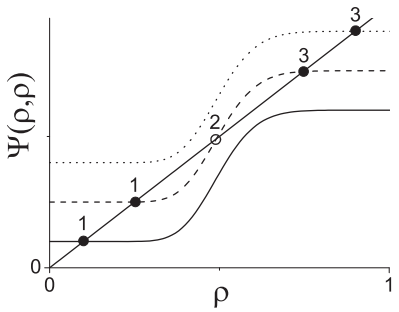

FIG. 1. Points 1, 2, and 3 represent solutions of the steady state equation $\rho = \Psi(\rho,\rho)$ for the cases $\langle n\rangle < n_{c1}$ (solid line), $n_{c1} < \langle n\rangle < n_{c2}$ (dashed line), and $\langle n\rangle > n_{c2}$ (dotted line).

C. Steady states

The shot noise intensity $\langle n\rangle$ determines activities ρ_e and ρ_i of excitatory and inhibitory populations at given model parameters. At zero fields $F_e = F_i = 0$, from Eqs. (6) we obtain $\rho_e = \rho_i \equiv \rho$ in a steady state ($d\rho_a/dt = 0$). ρ is a solution of the steady state equation

$$\rho = \Psi(\rho,\rho). \quad (8)$$

A graphical solution of the equation is displayed in Fig. 1. If the shot noise intensity $\langle n\rangle$ is either sufficiently small or large, then there is only one solution, either point 1 or point 3. These fixed points correspond to steady states with low and high neuronal activities, respectively. In an intermediate range $n_{c1} < \langle n\rangle < n_{c2}$, there are three fixed points (1, 2, and 3). The critical point $\langle n\rangle = n_{c1}$ is the point where fixed points 2 and 3 coalesce. Fixed points 1 and 2 coalesce at $\langle n\rangle = n_{c2}$. From Fig. 1, one sees that the coalescence occurs when

$$d\Psi(\rho,\rho)/d\rho = 1. \quad (9)$$

Together with the steady state equation (8), the condition (9) determines the critical points n_{c1} and n_{c2}.

While the fixed points depend on $\langle n\rangle$, but not on α, their local stability with respect to small perturbations depends on both $\langle n\rangle$ and α. It is determined by eigenvalues of the Jacobian of Eqs. (6),

$$\widehat{J}(\rho) = \begin{pmatrix} -1 + \partial\Psi/\partial\rho_e & \partial\Psi/\partial\rho_i \\ \alpha\partial\Psi/\partial\rho_e & -\alpha + \alpha\partial\Psi/\partial\rho_i \end{pmatrix}, \quad (10)$$

calculated at the fixed points. The eigenvalues are

$$\lambda_\pm = \tfrac{1}{2}(J_{11} + J_{22}) \pm \tfrac{1}{2}\sqrt{(J_{11} - J_{22})^2 + 4J_{12}J_{21}}, \quad (11)$$

where J_{ij} are the entries of the Jacobian. If $\lambda_\pm < 0$ at a fixed point, then this point is stable (attractor). If $\lambda_\pm > 0$, then the point is unstable. If one of the eigenvalues $\lambda_\pm$ is positive and

TABLE I. Local stability of the fixed points 1, 2, and 3 in the regions Ia–IIIb on the phase diagram in Fig. 2, where s = stable, sd = saddle, u = unstable, sp = spiral, lc = limit cycle.

	Ia	Ib	Ic	Id	Ie	IIa	IIb	IIIa	IIIb
1	s	s	s	s	s				
2		sd	sd	sd	sd				
3		s	s sp	u sp	u	s	s sp	u sp and lc	u and lc

the other is negative, then the point is saddle. If $\mathrm{Re}\lambda_\pm < 0$ and $\mathrm{Im}\lambda_\pm \neq 0$, the point is a stable spiral. If $\mathrm{Re}\lambda_\pm > 0$ and $\mathrm{Im}\lambda_\pm \neq 0$, the fixed point is an unstable spiral. The fixed points and their stability determine a phase portrait of Eqs. (6).

If the neuronal network is weakly perturbed from an equilibrium state corresponding to a stable fixed point ρ, then the real and imaginary parts of λ_+ at this point determine a relaxation rate γ_r to the state

$$\gamma_r = -\mathrm{Re}\lambda_+(\rho), \tag{12}$$

and the angular frequency γ_i of damped oscillations about the fixed point

$$\gamma_i = \mathrm{Im}\lambda_+(\rho). \tag{13}$$

D. Phase diagram

Analyzing the local stability of the fixed points 1, 2, and 3 in the $\alpha - \langle n\rangle$ plane (see Table I), we find the phase diagram of the cortical model displayed in Fig. 2. According to Table I, in regions Ia–Ie, the network relaxes exponentially to the stable fixed point 1 (of course, if a perturbation is small). In regions Ib and IIa, relaxation to the stable fixed point 3 is exponential while, in regions Ic and IIb, the relaxation occurs in the form of damped oscillations about the fixed point 3. In regions IIIa and IIIb, the fixed point 3 is an unstable point surrounded by a limit cycle. These are the regions with sustained network oscillations about the point 3. Nonlinear equations (6) have different phase portraits in phase regions Ia–IIIb in Fig. 2. The phase portraits in the (ρ_e,ρ_i) phase can be found by use of the standard methods [9,10]. They determine the patterns of collective neuronal activity and response of the network on stimuli.

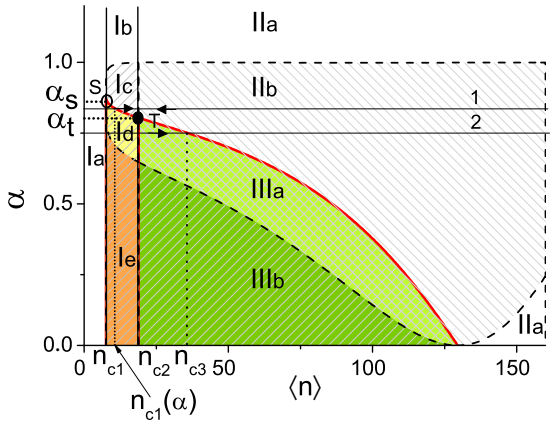

FIG. 2. (Color online) $\langle n\rangle - \alpha$ plane of the phase diagram of the cortical model. $\langle n\rangle$ is the shot noise intensity. α is the ratio of the response time of excitatory neurons to the response time of inhibitory neurons. The phase regions, the phase boundaries, and the parameters used in numerical calculations are explained in the text. The black dot represents the tricritical point T with the coordinate $\alpha_t \approx 0.80$. Lines 1 and 2 represent two scenarios discussed in the text.

In Fig. 2, the phase boundaries are represented by the dashed and solid lines. The vertical lines $\langle n\rangle = n_{c1}$ and $\langle n\rangle = n_{c2}$ are determined by the self-consistent solutions of Eqs. (8) and (9) discussed in Sec. II C. The boundaries between regions IIa and IIb and between regions IIIa and IIIb are determined by the condition

$$\gamma_i(\rho^{(3)}) = \mathrm{Im}\lambda_+(\rho^{(3)}) = 0 \tag{14}$$

(see the dashed lines in Fig. 2). The phase boundaries between regions Ic and Id and between regions IIb and IIIa are determined by the condition

$$\gamma_r(\rho^{(3)}) = -\mathrm{Re}\lambda_+(\rho^{(3)}) = 0 \tag{15}$$

(see solid line in Fig. 2). According to Eq. (15), on the boundary between regions IIb and IIIa, the relaxation rate is zero, i.e., critical slowing down occurs. The point $T = (n_{c2},\alpha_t)$ in Fig. 2 is a tricritical point of coexistence of three phases: the low activity state (regions Ic and Id), the high activity state (region IIb), and the state with sustained network oscillations (region IIIa). At the point T, the line of the first-order phase transition meets the lines of two continuous phase transitions. The point $S = (n_{c1},\alpha_s)$ is the common point of regions Ia, Ic, and Id. For the parameters used in our paper, we find $n_{c1} \approx 7.6$, $n_{c2} \approx 18.8$, $\alpha_s \approx 0.87$, and $\alpha_t \approx 0.80$.

We performed additional investigations of the cortical model with a small imbalance when $g_e J_e + g_i J_i \neq 0$ in the range $0.23 < g_i < 0.3$ around the balanced state at $g_i = 0.25$ (other model parameters were fixed). We found that the phase diagram is qualitatively the same as in the balanced state in Fig. 2. The critical point n_{c2} of the saddle-node bifurcation is almost constant in this range. With increasing g_i from 0.23 to 0.3, the region III with sustained network oscillations is broadening and the critical value α_t increases. At a given α, the critical point of the Hopf bifurcation n_{c3} is also monotonously increased as g_i increases from 0.23.

III. FIRST-ORDER PHASE TRANSITION

In this section, we study critical phenomena accompanying the first-order phase transition stimulated by shot noise. In particular, we study neuronal bursts and avalanches as precursors of the transition. Although bursts and avalanches have been broadly studied both experimentally and theoretically, understanding of their mechanism in the brain is elusive [2,20,24,25,54]. Here, apart from the standard measurements of the distribution function of avalanches over size, we also study critical behavior of the relaxation rate, a dependence of the power spectral density (PSD) of activity fluctuations on the shot noise intensity, and discuss finite-size effects. We find a dramatic increase of the zero-frequency peak of the PSD when the shot noise intensity tends to a critical point, while above the point the relaxation rate is nonzero and there are no critical fluctuations.

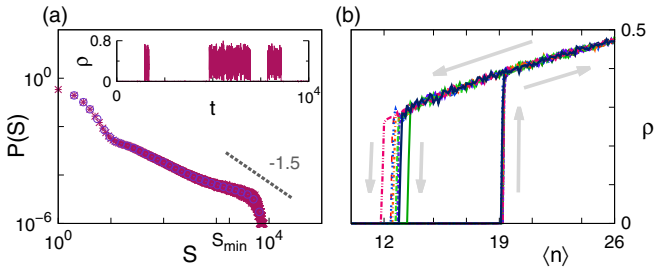

FIG. 3. (Color online) (a) Avalanche size distribution $P(s)$ versus size s at $\langle n\rangle = 18.8$ found by use of simulations ($N = 10^4$). The dashed line corresponds to $-\frac{3}{2}$ power law. $S_{\min}$ is explained in [57]. Inset: temporal activity of excitatory neurons near the first-order phase transition. Time t is in units of $1/\mu_e$. (b) Hysteresis in neuronal activity for increasing and decreasing noise level $\langle n\rangle$. In simulations, $\alpha = 0.85$.

The first-order phase transition occurs if $\alpha > \alpha_t$, i.e., when the response time T_i of an inhibitory neuron to stimulus is small enough in comparison with the response time T_e of an excitatory neuron. In simulations and numerical solution of Eqs. (6), we increased the noise level $\langle n\rangle$ from zero (region Ia) to a value in region IIa (or IIb) above the critical point n_{c2} and afterwards decreased it again to a value below n_{c2} (see line 1 in Fig. 2). When increasing the noise intensity $\langle n\rangle$, the neuronal activity undergoes a jump at $\langle n\rangle = n_{c2}$ [$n_{c2} \approx 18.8$ in Fig. 3(b)]. Therefore, the critical point n_{c2} is the limiting point of the first-order phase transition. This phase transition is caused by a saddle-node bifurcation that corresponds to coalescence of the stable point 1 and the saddle point 2. Simultaneously, at $\langle n\rangle = n_{c2}$, the eigenvalue $\lambda_+(\rho^{(1)})$ becomes zero while $\lambda_-(\rho^{(1)})$ remains to be negative. The first-order phase transition was also found in [21]. The line of the first-order phase transition ends up at the point (α_t, n_{c2}) on the phase diagram. If $\alpha < \alpha_t$, the neuronal networks undergoes a second-order phase transition at $\langle n\rangle = n_{c2}$ that will be discussed in Sec. IV.

A. Avalanches

In simulations, at $\langle n\rangle \leqslant n_{c2}$, we observe bursts of neuronal activity [see Fig. 3(a)]. When $\langle n\rangle \to n_{c2}$ the mean interburst interval decreases while the mean burst duration increases. The bursts are caused by avalanches (activation of a single neuron triggers activation of a cluster of neurons). These activation processes are stochastic. In our model, in networks of finite size, bursts are generated by finite-size fluctuations. We studied avalanches, analyzing spike time series by use of the standard method (see [24] or the recent work [55]). The avalanche size distribution $P(s)$ is represented in Fig. 3(a). Using the maximum likelihood estimate [56], we found that, when $\langle n\rangle$ is close to n_{c2}, the tail of $P(s)$ follows a power law $P(s) \propto s^{-z}$, with the exponent $z \approx 1.50$ and the corresponding p value is $p = 0.88$ (the closeness of p to 1 shows that the fit is good [57]). Our estimation is close to the value 1.62 obtained in [21]. Avalanches with the exponent z about 1.5 were also found near a saddle-node bifurcation in networks of leaky integrate-and-fire neurons with short-term synaptic depression [20]. Our estimation also agrees with experimental data [24,55] and the standard mean-field exponent $z = \frac{3}{2}$ obtained for other exactly solved models [42,58–62].

B. Hysteresis

At a given $\alpha > \alpha_t$, if $\langle n\rangle$ decreases from a value above n_{c2} to a value below n_{c2}, the network activity remains as high as it was above n_{c2} [see Fig. 3(b)]. The activity falls to a low value only at a critical intensity $\langle n\rangle = n_{c1}(\alpha)$, where $n_{c1} \leqslant n_{c1}(\alpha) \leqslant n_{c2}$. In the general case, $n_{c1}(\alpha)$ depends on α (see Fig. 2). If $\alpha > \alpha_s$, where α_s is the α coordinate of the point S on Fig. 2, hysteresis occurs in the range $n_{c1} < \langle n\rangle < n_{c2}$. If $\alpha_t < \alpha < \alpha_s$, hysteresis occurs in a smaller range of shot noise intensity $n_{c1}(\alpha) < \langle n\rangle < n_{c2}$ where $n_{c1}(\alpha)$ is the $\langle n\rangle$ coordinate of the interception point of the line 1 with the phase boundary between regions Ic and Id ending up at points S and T on the phase diagram in Fig. 2. The width of the hysteresis region, i.e, $n_{c2} - n_{c1}(\alpha)$, tends to zero when $\alpha \to \alpha_t$. At $\alpha < \alpha_t$, hysteresis is absent because, in regions Id and Ie, the fixed point 3 is unstable and there is only one stable fixed point 1. One notes that critical slowing down occurs at both limiting points of the first-order phase transition, i.e., at $\langle n\rangle = n_{c2}$ in the low activity state and at $\langle n\rangle = n_{c1}$ [or $n_{c1}(\alpha)$] in the high activity state. Hysteresis was observed, for example, in living neural networks [63] and in simulations of thalamocortical systems [64].

C. Critical slowing down of neuronal dynamics

For deeper understanding of the first-order phase transition, we now find analytically the relaxation rate to the low activity state. Writing Eq. (9) in the form $\partial\Psi/\partial\rho_e + \partial\Psi/\partial\rho_i = 1$ and substituting it into Eq. (11), we find that at $\langle n\rangle = n_{c2}$ the eigenvalue $\lambda_+(\rho^{(1)})$ is zero at the fixed point 1. Therefore, the relaxation rate [Eq. (12)] to the low activity state is also zero:

$$\gamma_r = -\lambda_+(\rho^{(1)}) = 0. \tag{16}$$

This phenomenon is so-called critical slowing down. Note that it takes place on the line $\langle n\rangle = n_{c2}$ at all α, both above and below α_t (see Fig. 2).

We now find dependence of the relaxation rate γ_r on $\langle n\rangle$ at $0 < n_{c2} - \langle n\rangle \ll n_{c2}$. We use the Taylor expansion of λ_+ over small $\delta\rho \equiv \rho^{(1)}(n_{c2}) - \rho \ll \rho^{(1)}(n_{c2})$ in Eq. (11) and obtain

$$\lambda_+(\rho) = \lambda_+[\rho^{(1)}(n_{c2})] + \frac{d\lambda_+(\rho)}{d\rho}\delta\rho + \dots . \tag{17}$$

The first term is zero. Using Eq. (A2) for $\delta\rho$ from Appendix A, in the leading order, we obtain

$$\gamma_r = -\lambda_+(\rho) \propto (n_{c2} - \langle n\rangle)^{1/2}. \tag{18}$$

This behavior occurs both at $\alpha > \alpha_t$ and $\alpha < \alpha_t$.

If a neuronal network has a finite but large size $N \gg 1$, then according to the scaling law hypothesis, near a critical point n_c of a continuous phase transition, the relaxation rate γ_r is described by the general scaling law

$$\gamma_r(\langle n\rangle, N) = (\langle n\rangle - n_c)^{\sigma} X[(\langle n\rangle - n_c)N^{1/\nu}] \tag{19}$$

with a scaling function $X(x)$ and exponents σ and ν which can be found by use of renormalization group techniques [23,65,66]. One assumes that the scaling law also is valid

near the limiting point n_{c2} of the first-order phase transition [59]:

$$\gamma_r(\langle n\rangle, N) \propto (\langle n\rangle/n_c - 1)^{\sigma}, \text{ if } N^{-1/\nu} \ll \langle n\rangle/n_c - 1 \ll 1$$
$$\propto N^{-\sigma/\nu}, \quad \text{if} \quad \langle n\rangle/n_c - 1 \ll N^{-1/\nu} \qquad (20)$$

where $\sigma = \frac{1}{2}$. Thus, at a finite but large size $N \gg 1$, the relaxation rate γ_r is nonzero at any $\langle n\rangle$ due to finite-size effects that smear the critical singularity. This agrees with results of our simulations presented in the following section.

D. Power spectral density of fluctuations near the first-order phase transition

We now find the power spectral density (PSD) of activity fluctuations in the low activity state when $\langle n\rangle$ is close to n_{c2}. In simulations, we measured the PSD of excitatory and inhibitory activities. We also solved analytically Eqs. (6) with weak white-noise forces $F_e(t)$ and $F_i(t)$, where $F_e(t), F_i(t) \propto 1/\sqrt{N}$. The forces mimic forces caused by finite-size effects (this method was also used in [14]). Our calculations are represented in Appendix B. We find that, in the low activity state, the PSD defined as

$$S(\omega) \equiv \langle \delta\rho_e(\omega)\delta\rho_e(-\omega)\rangle, \qquad (21)$$

where $\delta\rho_e(t) \equiv \rho_e(t) - \rho^{(1)}$, has a sharp zero frequency peak described by the following shape function [see Eq. (B8)]:

$$\frac{S(\omega)}{S_{\max}} \approx \frac{1}{(\omega/\gamma_r)^2 + 1}. \qquad (22)$$

The peak maximum is $S_{\max} \propto 1/\gamma_r^2$. Figure 4(a) displays the PSD $S(\omega)$ measured in our simulations in the low activity state in region Ic. In Fig. 4(b), we compare simulations with the theoretical prediction. One sees that Eq. (22) describes well the measured frequency dependence of the PSD. According to Eq. (18), at $\langle n\rangle \to n_{c2}$, the peak maximum increases as

$$S_{\max} \propto 1/(n_{c2} - \langle n\rangle). \qquad (23)$$

Our simulations support the predicted increase of the zero-frequency peak $S_{\max}$ [see the inset in Fig. 4(b)]. When $\langle n\rangle$ is close to n_{c2}, finite-size effects [Eq. (20)] become important and γ_r remains nonzero, although very small, even at the critical point. As a result, $S_{\max}$ has a maximum at $\langle n\rangle = n_{c2}$ instead of divergency. The numerical results also confirm the linear decrease of $1/S_{\max}$, $1/S_{\max} \propto n_{c2} - \langle n\rangle$, predicted by Eq. (23) when $\langle n\rangle \to n_{c2}$. In contrast, $S_{\max}$ has no maximum at n_{c2} when $\langle n\rangle$ tends to n_{c2} from the high activity state (it is the manifestation of hysteresis).

The Lorentzian behavior of the PSD of synaptic currents has been observed in cat cortex during wakefulness [67]. In Ref. [67], it was suggested that this behavior may be driven by a white-noise process. During slow-wave sleep, the PSD deviates from the Lorentzian [67]. This deviation suggests that, in a general case, stochastic forces may be statistically different from white noise.

Thus, the cortical model shows that bursts and avalanches appear near the limiting point of metastable states of the first-order phase transition caused by a saddle-node bifurcation in agreement with other network models [20,21,58,59]. Critical phenomena (power-law statistics for avalanches and sharp zero-frequency peak of the PSD) due to critical slowing down in the low activity state (when approaching the critical point from below), the absence of the critical phenomena above the point (because, in the high activity state, the relaxation rate is nonzero at the critical point) and hysteresis are the characteristic properties of the first-order phase transition, which can be experimentally tested.

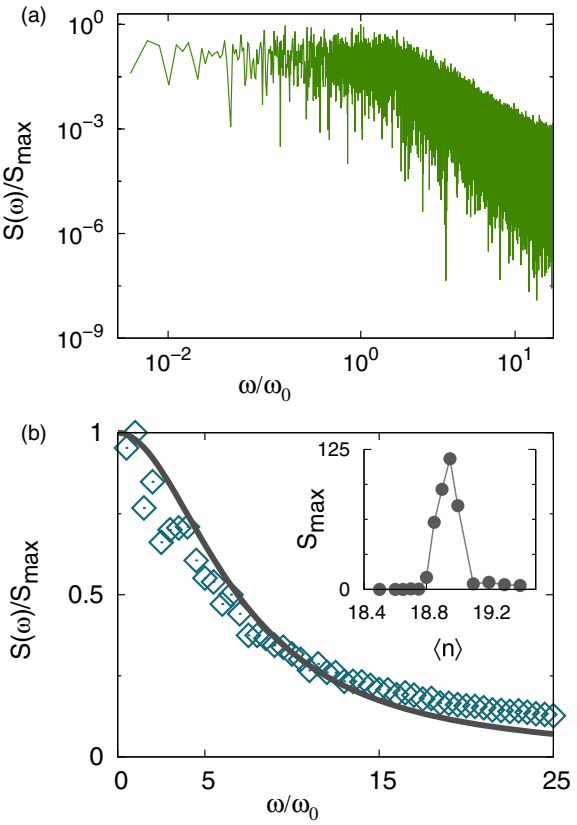

FIG. 4. (Color online) (a) Power spectral density $S(\omega)$ of activity fluctuations versus frequency ω in the low activity state of the cortical model (results of simulations at the shot noise intensity $\langle n\rangle = 18.7$, $\alpha = 0.85$). (b) Averaged frequency dependence of $S(\omega)$ at small frequencies. Results of simulations are shown by open diamonds. The solid line represents Eq. (22) with $\gamma_r = 6.9(2)$ and $\omega_0 = 0.03$. Frequencies are in units of μ_e. Inset: the zero-frequency peak $S_{\max} = S(\omega = 0)$ versus $\langle n\rangle$ when increasing $\langle n\rangle$. The observation time was $10\,000/\mu_e$.

Another mechanism of avalanches based on ideas of self-organized criticality by Per Bak [68] is discussed in [2]. From our point of view, at the present time, there is no direct experimental evidence that supports one approach over the other. Further experimental and theoretical investigations of these two approaches are necessary for understanding avalanches in the brain.

IV. SECOND-ORDER NONEQUILIBRIUM PHASE TRANSITIONS

We now consider the case $\alpha < \alpha_t$, i.e., when excitatory neurons respond faster on stimuli compared to inhibitory neurons. We show that, when increasing the shot noise intensity, the cortical model undergoes successively two second-order

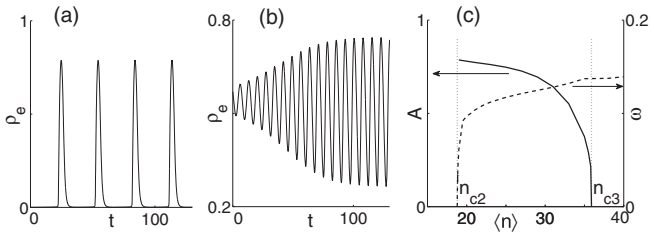

FIG. 5. Network oscillations near (a) the saddle-node ($\langle n\rangle = 18.805$, $n_{c2} = 18.8$) and (b) supercritical Hopf ($\langle n\rangle = 34$, $n_{c3} = 36$) bifurcations. (c) Amplitude (solid line) and frequency (dashed line) of network oscillations versus $\langle n\rangle$. At $\langle n\rangle > n_{c3}$, the oscillations are damped. These results are obtained from numerical integration of Eqs. (6). Time t is in units of $1/\mu_e$, and $\alpha = 0.75$.

phase transitions. We find that sustained network oscillations emerge at a saddle-node bifurcation and disappear at a Hopf bifurcation. We study properties of the phase transitions, critical phenomena, patterns of spontaneous activity, and sustained network oscillations near the critical intensities of shot noise.

A. Saddle-node bifurcation

At a given $\alpha < \alpha_t$, we increase shot noise intensity $\langle n\rangle$ from $\langle n\rangle = 0$ (see line 2 in Fig. 2). The neuronal network goes from region Ia with the single fixed point 1 into region Id or Ie where its dynamics is determined by three fixed points: the stable point 1, the saddle point 2, and the unstable point 3 (see Table I). At $\langle n\rangle = n_{c2}$, the points 1 and 2 coalesce and the network undergoes a second-order phase transition due to a saddle-node bifurcation from a state with a low activity and short-range temporal correlations between neurons into a state with regular sustained network oscillations (regions IIIa or IIIb). In regions IIIa and IIIb, dynamics of neuronal networks is determined by the unstable fixed point 3 surrounded by a limit cycle. At $\langle n\rangle > n_{c2}$, the network oscillations emerge with a large amplitude [see Fig. 5(a)] and their frequency increases from zero as $\omega \propto (\langle n\rangle - n_{c2})^{1/2}$ [see Fig. 5(c)]. This frequency dependence is a very general feature of oscillations in nonlinear dynamic systems close to the saddle-node bifurcation [9,11,12]. Note, however, that in our model, we deal with a phase transition, i.e., a collective phenomenon in neuronal networks. We suggest that for this kind of continuous phase transition the frequency is the order parameter.

In simulations, at $\langle n\rangle$ below n_{c2}, we observed irregular almost identical sharp spikes of neuronal activity [see Fig. 6(a)]. The mean frequency of the spikes is very small and increases when the shot noise intensity tends to the critical point n_{c2} while the spike duration is almost constant and much larger than the period $(1/f)$ of oscillations generated by a single neuron. This kind of activity differs sharply from bursts found near the first-order phase transition (compare Figs. 3 and 6). The sharp spikes emerge from a low background activity with a rapid onset [Fig. 6(b)]. They reach a large amplitude, involve in synchronized activity about 90% of neurons, and end up with an abrupt return to lower activity. In Fig. 6, the spike duration is about 90 ms and the mean interspike interval is about 34 s at $1/\mu_e = 20$ ms.

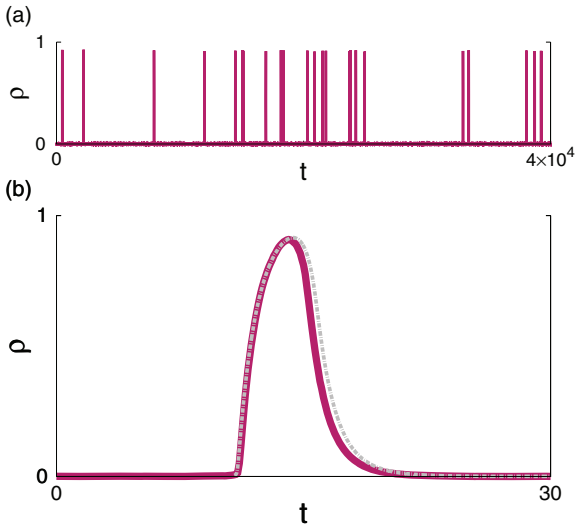

FIG. 6. (Color online) (a) Series of sharp spikes of neuronal activity near the saddle-node bifurcation. (b) Paroxysmal-like spike of activity. Solid and dashed lines represent spikes found in simulations and numerical integration of Eqs. (6), respectively. Parameters: shot noise intensity $\langle n\rangle = 18.76$ and $\alpha = 0.55$. Time t is in units of $1/\mu_e$.

In order to understand the mechanism of generation of the sharp spikes, we performed numerical integration of Eqs. (6) with nonzero stochastic forces F_e and F_i representing finite-size effects at the same parameters as in simulations. The numerical integration also reveals sharp spikes that are identical to those observed in simulations [Fig. 6(b)]. Our analysis of the phase portrait of Eqs. (6) in regions Id and Ie shows that the sharp spikes are strongly nonlinear events in neuronal activity generated by fluctuations. In the (ρ_i, ρ_e) phase plane, their trajectories are topologically equivalent to the heteroclinic orbits found in the Morris-Lecar model (see Fig. 7.4 in Ref. [11]).

Analyzing properties of the sharp spikes, such as emergence conditions, course of the events, their shape, amplitude, duration, and low frequency oscillations, we find that this kind of spontaneous neuronal activity is similar to such epileptiform activity as the paroxysmal spikes observed in EEG activity [26,27]. Based on this similarity we suggest that the paroxysmal spikes and other seizurelike events, such as slow-wave oscillations [27] or sharp waves in hippocampus [3,28], are possible strongly nonlinear waves appearing in neuronal networks near a saddle-node bifurcation. Of course, in order to describe in detail the events, a realistic network structure and realistic single-neuron dynamics must be taken into account.

At $\langle n\rangle$ below n_{c2}, the relaxation rate γ_r is $\gamma_r \propto (n_{c2} - \langle n\rangle)^{1/2}$ [Eq. (18)]. This result is in contrast to the standard mean-field theory (the Landau theory) that predicts $\gamma_r \propto |n_{c2} - \langle n\rangle|$ for a second-order phase transition. The nonstandard scaling behavior and emergence of paroxysmal-like spikes near the saddle-node bifurcation show an unusual character of the phase transition. Our simulations and numerical integration also reveal an almost constant nonzero time lag Δt_l between excitatory and inhibitory activities at $\langle n\rangle$ around n_{c2}.

For the spike in Fig. 6, inhibitory activity reaches a maximum 11 ms after excitatory activity.

In the context of stochastic resonance, several nonlinear dynamical systems [69–71] and single-neuron models [71–73], which have excitable dynamics of the same kind as the Morris-Lecar model and our cortical model, have been considered. Phase transitions triggered by a saddle-node bifurcation into a state with sustained large-amplitude oscillations were also found in complex physical and chemical systems such as the system of limit-cycle oscillators with all-to-all coupling [74] and CO oxidation on the Pt(110) surface [75]. However, critical phenomena and single nonlinear oscillations preceding the transition were not studied. As far as we know, paroxysmal-like spikes as collective nonlinear objects were not studied within a neuronal network model. A detailed investigation of the nature and mechanism of generation of the paroxysmal-like spikes will be published elsewhere.

B. Supercritical Hopf bifurcation

We now study the second-order phase transition due to the supercritical Hopf bifurcation. For this purpose, we perform simulations of the cortical model, numerical integration, and analytical analysis of Eqs. (6). We find critical behavior and demonstrate a difference in critical properties between the saddle-node and supercritical Hopf bifurcations.

When increasing the shot noise intensity $\langle n\rangle$ above n_{c2}, the frequency of sustained oscillations increases while their amplitude decreases [see Fig. 5(c)]. The oscillations disappear at a critical noise intensity $\langle n\rangle = n_{c3}$ which depends on α (see the line 2 in Fig. 2). At $\langle n\rangle = n_{c3}$, the network undergoes a phase transition from a state with the unstable point 3 surrounded by a limit cycle (region IIIa) into a state in which the fixed point 3 is a stable spiral (region IIb). From the stability analysis in Sec. II C, it follows that this transition is due to the supercritical Hopf bifurcation. Above n_{c3}, the network enters region IIb with damped network oscillations about the fixed point 3. Note also that network oscillations taking place near the saddle-node and supercritical Hopf bifurcations have different patterns [compare Figs. 5(a) and 5(b)]. Oscillations emerging due to a Hopf bifurcation were also found in a stochastic rate model [22].

1. Neuronal activity below the Hopf bifurcation

First, we study sustained network oscillations at $\langle n\rangle$ below n_{c3}. We expand $\Psi(\rho_e,\rho_i)$ in Eqs. (6) in a series in $\delta\rho_a(t) \equiv \rho_a(t) - \rho^{(3)}$ around the fixed point 3 and hold terms up to $O(\delta\rho_a^3)$ inclusively. Then, we solve Eqs. (6) in region IIIa, using the averaging theory [9]. Details of our calculations are in Appendix C. When $\langle n\rangle \to n_{c3}$, we find a decrease of the oscillation amplitude A,

$$A \propto (n_{c3} - \langle n\rangle)^{1/2}, \tag{24}$$

and a decrease of the relaxation rate γ_r^*,

$$\gamma_r^* \propto n_{c3} - \langle n\rangle. \tag{25}$$

Note that relaxation rate γ_r^* characterizes relaxation of perturbed neuronal activity to sustained network oscillations, for example, relaxation of network oscillations with a perturbed amplitude to oscillations with a steady amplitude [this process is shown in Fig. 5(b)]. γ_r^* can be found from a solution of nonlinear dynamical equations (see Appendix D). γ_r^* differs from the parameter γ_r calculated at the fixed point 3. At $\langle n\rangle < n_{c3}$, $\gamma_r(\rho^{(3)})$ is negative and determines runaway of the neuronal activity from the unstable fixed point 3 [this process is represented by the initial increase of the oscillation amplitude in Fig. 5(b)]. $\gamma_r(\rho^{(3)})$ is positive and plays the role of relaxation rate only at $\langle n\rangle > n_{c3}$.

In Appendix D, it is shown that, at $\langle n\rangle < n_{c3}$, a phase lag $\Delta\varphi$ between synchronized activities of excitatory and inhibitory populations is

$$\Delta\varphi \propto n_{c3} - \langle n\rangle. \tag{26}$$

$\Delta\varphi$ determines the time lag $\Delta t_l = \Delta\varphi/\gamma_i$ between maximums of excitatory and inhibitory activities. At $\langle n\rangle = n_{c3}$, $\Delta\varphi$ and Δt_l are zero which means a strict synchronization between excitatory and inhibitory activities. This is in contrast to an always finite time lag in the case of the saddle-node bifurcation.

Thus, Eqs. (24)–(26) show that, when the noise intensity $\langle n\rangle$ tends to the critical point n_{c3} of the supercritical Hopf bifurcation, the phase transition is signaled by a decrease of the oscillation amplitude A, the relaxation rate γ_r^*, and the time lag Δt_l. At $\langle n\rangle = n_{c3}$, γ_r^* is zero which manifests the critical slowing down. The amplitude A is the order parameter for the phase transition. These phenomena are general features of the supercritical Hopf bifurcation. Comparing Eq. (25) with (18) and the behavior of the time lag Δt_l at $\langle n\rangle = n_{c2}$ and $\langle n\rangle = n_{c3}$, we conclude that the continuous phase transitions corresponding to the saddle-node and supercritical Hopf bifurcations have different critical behaviors and, therefore, belong to different classes of universality.

2. Neuronal activity above the Hopf bifurcation

We now analyze analytically the critical behavior of the cortical model at $\langle n\rangle$ above n_{c3}. Our simulations show that, above n_{c3}, spontaneous activity has a form of spindle oscillations (see the inset in Fig. 7). The spindle oscillations are similar to spindles observed, for example, in thalamus [30]. Damped oscillations were observed in an instance of epilepsy (see, for example, [76]). If $\langle n\rangle$ tends to n_{c3} from above, then the amplitude of spindle oscillations increases while the relaxation rate γ_r tends to zero as $\gamma_r \propto \langle n\rangle - n_{c3}$ according to Eq. (C8) in Appendix C. This results in an increase of the peak of the power spectral density of activity fluctuations at the frequency of damped oscillations (see Fig. 7). Moreover, the phase lag $\Delta\varphi$ between synchronized activities of excitatory and inhibitory populations also tends to zero as $\Delta\varphi \propto \langle n\rangle - n_{c3}$ according to Eq. (D4). These critical phenomena signal an approach to the Hopf bifurcation. In order to understand the phenomena, we use simulations and analytical calculations. According to Appendix B 2, the PSD, $S(\omega)$, has a resonance peak

$$S(\omega)/S_{\max} \approx 4\zeta^2/[(1-x^2)^2 + 4\zeta^2 x^2], \tag{27}$$

where $x = \omega/\omega_0$ and $\omega_0 \equiv \sqrt{\gamma_r^2 + \gamma_i^2}$. The parameter ζ,

$$\zeta \equiv \gamma_r/\omega_0, \tag{28}$$

is the damping ratio of damped oscillations. The peak maximum is $\max S(\omega) \equiv S_{\max} \propto 1/\zeta^2$. This behavior of $S_{\max}$ is due to the fact that the amplitude of damped oscillations increases

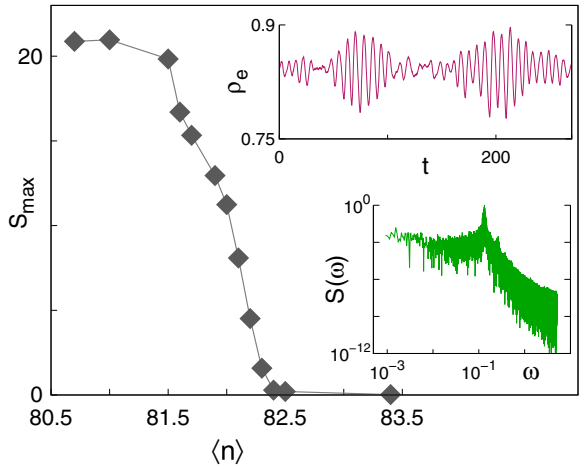

FIG. 7. (Color online) The peak maximum S_{max} of the power spectral density (PSD) of fluctuations versus $\langle n\rangle$ above the supercritical Hopf bifurcation (in simulations, $\langle n\rangle > n_{c3} \approx 80.5$ and $\alpha = 0.55$). Inset: temporal neuronal activity in the form of spindles and the PSD $S(\omega)$ versus the frequency ω at $\langle n\rangle = 82.5$. Time t is in units of $1/\mu_e$.

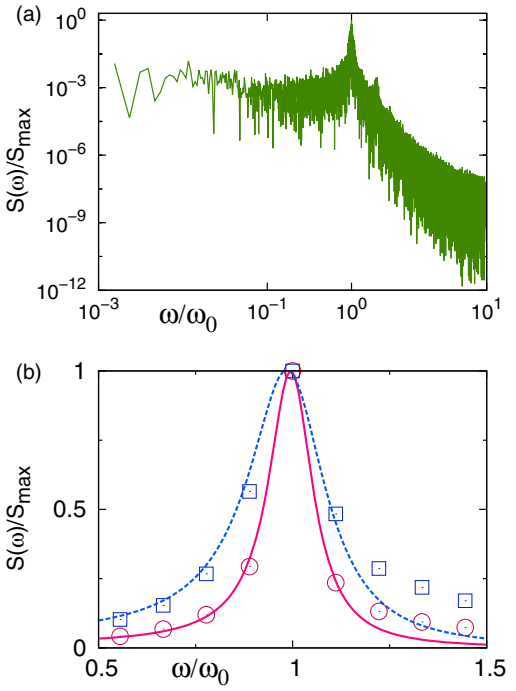

FIG. 8. (Color online) (a) Power spectral density (PSD) $S(\omega)$ of activity fluctuations above the supercritical Hopf bifurcation for $\alpha = 0.55$ (from simulations). (b) Averaged frequency dependence of $S(\omega)$ around the peak at $\omega_0 = 0.15$: the PSD at $\langle n\rangle = 85$ (blue open rectangles); the analytical calculation from Eq. (27) with $\gamma_r = 0.12(1)$ (blue dashed line); the PSD at $\langle n\rangle = 82.5$ (pink open circles); the analytical calculation from Eq. (27) with $\gamma_r = 0.069(4)$ (pink solid line). Frequencies are in units of μ_e.

as $A \propto 1/\zeta \propto 1/(\langle n\rangle - n_{c3})$ when $\langle n\rangle \to n_{c3}$ [see Eq. (B12)]. In turn, the amplitude decreases when $\langle n\rangle$ increases and the network goes away from the supercritical Hopf bifurcation. Note that the relaxation rate γ_r determines the time decay of the damped oscillations and can be found from data analysis of a time dependence of the autocorrelation function [Eqs. (B2) and (B12)]. From this analysis, one finds the dimensionless parameter ζ that is an important characteristic of the closeness of the network to the critical point n_{c3}. The smaller is ζ the closer is the network to the critical point. In the infinite-size limit, ζ is zero at $\langle n\rangle = n_{c3}$. A similar resonance peak of the PSD was also found within the integrate-and-fire model in [15–17].

In Fig. 8, we represent the PSD of activity fluctuations measured in simulations. In agreement with the theoretical prediction, the measured PSD, $S(\omega)$, reveals a sharp maximum at the frequency of damped oscillations. Figure 7 shows that, when $\langle n\rangle \to n_{c3}$, the maximum value S_{max} first strongly increases and then saturates at a certain value due to the finite-size effects [Eq. (20)]. Figure 8 shows that the shape of this maximum is well described by the shape function (27).

The critical behavior of the cortical model near the supercritical Hopf bifurcation helps to understand the attenuation of alpha rhythms by visual or auditory stimuli (the Berger effect) [77,78]. Recall that the Berger effect manifests itself in activation of alpha waves on the electroencephalogram when the eyes are closed and diminution of alpha waves when they are opened (see, for example, the review of [77]). Based on the cortical model, we suggest that opening eyes may result in an increase of the flow of spikes bombarding neurons in the area of the cortex that is responsible for the alpha waves. As a result, the neuronal network goes away from the Hopf bifurcation and the amplitude of damped oscillations decreases. A similar phenomenon was also observed in the auditory cortex where the tau rhythm (the tau rhythm belongs to the family of alpha rhythms) was transiently suppressed by auditory stimuli [78].

C. Similarity between the cortical model and the Morris-Lecar model

Above, we discussed local stability of fixed points and bifurcations of nonlinear equations (6) in the cortical model in dependence on the shot noise intensity and the parameter α. Based on these results, one builds phase portraits of Eqs. (6). In the case $\alpha < \alpha_t$, we revealed that the phase portraits in regions Id, Ie, IIIa, and IIIb are topologically equivalent (in other words, homeomorphic) to the phase portraits found in the Morris-Lecar model stimulated by an applied current in the case when the I-V relation is N shaped [11]. Recall that the Morris-Lecar model is a simplified version of the four-dimensional Hodgkin-Huxley model. Within the Morris-Lecar model, a system of two nonlinear equations describes a relationship between the membrane potential and the activation of K^+ ion channels within the membrane. It is well known that the topological equivalence of phase portraits of two dynamical systems results in similar dynamics and similar responses on stimuli [10]. Therefore, the dynamic behavior of the cortical model stimulated by shot noise (a flow of random spikes bombarding neurons) must be similar in some respects to the dynamic behavior of the Morris-Lecar model stimulated by an applied current. In this case, we can apply results obtained for the well-studied Morris-Lecar model to the cortical model. Izhikevich [12] showed that the Morris-Lecar neuron acts as an "integrator," when it is close

to the saddle-node bifurcation, and as a "resonator," when it is close to the Hopf bifurcation. Based on the topological equivalence, we can conclude that the cortical model acts in a similar way near the bifurcations. Indeed, in Sec. IV A, we showed that if the mean frequency of incoming random spikes is a little bit larger than the critical frequency corresponding to the saddle-node bifurcation, then a neuronal network oscillates with an arbitrary low frequency. The higher the mean frequency of incoming random spikes, the higher the frequency of sustained network oscillations. Thus, we can say that the network acts as an integrator. In contrast, when the network is in the rest state near the supercritical Hopf bifurcation, it acts as a resonator because it responds preferentially to a certain (resonant) frequency of input (see Sec. IV B). Furthermore, in Sec. IV A, the topological equivalence helped us to understand the nature of paroxysmal-like spikes observed near the saddle-node bifurcation because similar nonlinear spikes were found in the Morris-Lecar model [11].

V. CONCLUSION

In conclusion, within an exactly solvable cortical model of neuronal networks with stochastic excitatory and inhibitory neurons, we studied first- and second-order phase transitions stimulated by shot noise (a flow of random spikes bombarding neurons). We performed simulations, numerical integration, and analytical analysis of nonlinear dynamical equations. These methods gave results in complete agreement with each other. The advantage of our model is that it gives a possibility to study both noise-induced first- and second-order phase transitions in neuronal networks by use of a unified approach and standard physical and mathematical methods. This unified approach allowed us to compare qualitatively and quantitatively critical phenomena accompanying the phase transitions, patterns of spontaneous neuronal activity, and their dependence on the shot noise intensity. Furthermore, the rate equations derived for the model allowed us to study strongly nonlinear events, such as paroxysmal-like spikes and slow waves observed in neuronal activity, that can not be described by a linear theory. Our results support the idea that collective behavior of neuronal networks may have universal properties that do not depend on details of single-neuron dynamics. The universal collective phenomena are determined by general properties of neuronal networks, such as the network structure, balance between excitatory and inhibitory neurons, the presence of noise, and interaction between neurons.

We showed that if inhibitory neurons respond faster to stimuli than excitatory neurons, then a first-order phase transition manifests itself as a jump from low to high neuronal activity at a critical noise intensity. We found the mechanism of the transition and showed that it occurs due to a saddle-node bifurcation. We studied in detail critical phenomena that accompany the transition and patterns of spontaneous activity near the critical point. In particular, we showed that bursts and avalanches are precursors of the first-order phase transition. When the shot noise intensity tends to the limiting point of the metastable states, then the size distribution of neuronal avalanches becomes a power law with the exponent about 1.5. Moreover, at the critical point, critical slowing down occurs in the infinite network, i.e., the relaxation rate is zero at the critical noise intensity. Our simulations revealed that finite-size effects smear the phase transition and make the relaxation rate to be nonzero at the critical point. Critical phenomena (power-law statistics for avalanches and sharp zero-frequency peak of the PSD) due to critical slowing down in the low activity state (when approaching the critical point from below), the absence of the critical phenomena above the point (because, in the high activity state, the relaxation rate is nonzero at the critical point), and hysteresis are the characteristic properties of the first-order phase transition, which can be experimentally tested.

We also studied two noise-induced second-order phase transitions that occur if inhibitory neurons respond slower to stimuli than excitatory neurons. These transitions represent two scenarios of appearance and disappearance of network oscillations. When increasing the shot noise intensity, at first, sustained network oscillations appear due to a saddle-node bifurcation, and then, at a higher shot noise intensity, the oscillations disappear due to a supercritical Hopf bifurcation. Our analysis showed that the continuous phase transitions caused by the saddle-node and supercritical Hopf bifurcations are accompanied by different critical phenomena and different patterns of spontaneous neuronal activity. The transitions are characterized by different order parameters and belong to different classes of universality.

We analyzed patterns of spontaneous neuronal activity near the saddle-node and Hopf bifurcations. Our most interesting result is the observation of paroxysmal-like spikes that precede the second-order phase transition caused by the saddle-node bifurcation. We found that the spikes are strongly nonlinear objects that appear instantly from a low background activity with a rapid onset, reach a large amplitude, involve in synchronized activity about 90% of neurons, and end up with an abrupt return to lower activity. These spikes are similar to single paroxysmal spikes and sharp waves observed in EEG measurements. With increasing the shot noise intensity above the critical point of the saddle-node bifurcation, low frequency network oscillations follow the irregular spikes. They appear with a large amplitude but a small frequency (at the critical point, the frequency is zero). The pattern of the oscillations resembles sharp-slow waves [27] or sharp waves in hippocampus [3,28,29]. In contrast to the saddle-node bifurcation, spontaneous activity above the Hopf bifurcation is represented by irregular spindles formed by damped oscillations. Sustained network oscillations below the supercritical Hopf bifurcation have a small amplitude (at the critical point, the amplitude is zero in the infinite-size limit) and a finite frequency. These oscillations are also nonlinear and have properties such as those of the Van der Pol oscillator.

We also analyzed the power spectral density (PSD) of spontaneous neuronal activity near the critical points of the phase transitions. We showed that the frequency dependence of the PSD and its dependence on the shot noise intensity give a rich information about the kind of bifurcation and the closeness of the network to the critical point. In particular, the PSD has a zero-frequency peak near the first-order phase transition, while above the supercritical Hopf bifurcation the PSD has a peak at the frequency of damped oscillations. The peaks are strongly enhanced when the noise intensity tends to the critical points of the phase transitions. These results may be

applied to an analysis of spectral properties of EEG recording in order to predict an approach to a critical point in neuronal activity.

Finally, we discussed an amazing similarity between excitability of the considered cortical model stimulated by shot noise and excitability of the Morris-Lecar neuron stimulated by an applied current [11,12,33]. This similarity results from the fact that the cortical model of neuronal networks and the Morris-Lecar model have topologically equivalent phase portraits. This similarity allowed us to conclude that a neuronal network acts as "integrator" when it is close to the saddle-node bifurcation, and as a "resonator" when it is close to the supercritical Hopf bifurcation. We believe this similarity may be useful for understanding many nonlinear phenomena in dynamics of neuronal networks.

In our model, a flow of random spikes bombarding neurons represents a combined effect of synaptic noise (spontaneous release of neurotransmitters), stimuli from other brain areas, and sensory stimuli. At given model parameters, the flow controls dynamics of the neuronal network. If the flow intensity is close to a critical value, then even a small change in the flow intensity can switch the network from one to another state. In other words, a small change of activity of neuronal networks to which a considered network is connected may strongly impact on a dynamic state of the network under consideration. This represents one of the important mechanisms of interaction between neuronal networks [79].

ACKNOWLEDGMENTS

We thank S. N. Dorogovtsev for stimulating discussions. This work was partially supported by FET IP Project No. MULTIPLEX 317532 and by the PTDC Projects No. SAU-NEU/103904/2008, No. FIS/108476/2008, No. MAT/114515/2009, Project No. PEst-C/CTM/LA0025/2011, and the project "New Strategies Applied to Neuropathological Disorders," cofunded by QREN and EU. K.E.L. and M.A.L. were supported by the FCT Grants No. SFRH/BPD/71883/2010 and No. SFRH/BD/68743/2010.

APPENDIX A: NEURONAL ACTIVITY NEAR THE CRITICAL POINTS

Let us find the activity $\rho^{(1)}$ in the low activity state near the critical point $\langle n\rangle = n_{c2}$ of the saddle-node bifurcation, i.e., at $0 < n_{c2} - \langle n\rangle \ll n_{c2}$. In simulations, $\rho^{(1)}$ can be found by measuring neuronal activity $\rho_e(t)$ and averaging it over a sufficiently large observation time. In Eq. (8), we use the Taylor expansion of the function $\Psi(\rho,\rho)$ over $\varepsilon \equiv \langle n\rangle - n_{c2}$ and $\delta\rho \equiv \rho - \rho^{(1)}(n_{c2})$ up to the second order in $\delta\rho$. Then, Eq. (8) takes a form

$$\delta\rho = \frac{\partial\Psi}{\partial\langle n\rangle}\varepsilon + \frac{d\Psi}{d\rho}\delta\rho + \frac{1}{2}\frac{d^2\Psi}{d\rho^2}(\delta\rho)^2 + \ldots, \tag{A1}$$

where the function Ψ and its derivatives are calculated at $\langle n\rangle = n_{c2}$. Using Eqs. (8) and (9), we find a solution

$$\delta\rho = \rho^{(1)} - \rho^{(1)}(n_{c2}) \approx -K(n_{c2} - \langle n\rangle)^{1/2}, \tag{A2}$$

where

$$K = \left|2\frac{\partial\Psi}{\partial\langle n\rangle}\Big/\frac{d^2\Psi}{d\rho^2}\right|^{1/2}. \tag{A3}$$

The singular behavior (A2) is a general attribute of hybrid and first-order phase transitions [60–62]. Note that $\rho(\langle n\rangle)$ near the fixed point 2 is

$$\rho^{(2)}(\langle n\rangle) - \rho^{(1)}(n_{c2}) \approx K(n_{c2} - \langle n\rangle)^{1/2} \tag{A4}$$

because, at $\langle n\rangle = n_{c2}$, the points 1 and 2 coalesce and $\rho^{(1)}(n_{c2}) = \rho^{(2)}(n_{c2})$.

Neuronal activity $\rho = \rho^{(3)}(\langle n\rangle)$ near the Hopf bifurcation can be found at $0 < \langle n\rangle - n_{c3} \ll n_{c3}$ by use of the Taylor expansion (A1) with $\varepsilon \equiv \langle n\rangle - n_{c3}$ and $\delta\rho \equiv \rho - \rho^{(3)}(n_{c3})$, where the function Ψ and its derivatives are calculated at $\langle n\rangle = n_{c3}$. In this case, the linear terms give the leading contribution to a solution

$$\rho^{(3)}(\langle n\rangle) - \rho^{(3)}(n_{c3}) \approx \frac{\partial\Psi}{\partial\langle n\rangle}\frac{\langle n\rangle - n_{c3}}{(1 - d\Psi/d\rho)}, \tag{A5}$$

in contrast to the square root dependence in Eq. (A2).

APPENDIX B: POWER SPECTRAL DENSITY OF ACTIVITY FLUCTUATIONS

The power spectral density (PSD) of fluctuations of neuronal activity encodes rich information about critical phenomena. According to the Wiener-Khintchine theorem, the power spectral density $S(\omega)$ of activity fluctuations of the excitatory population is the Fourier transform of the autocorrelation function $C_{ee}(t)$:

$$S(\omega) = \frac{1}{2\pi}\int_{-\infty}^{\infty} e^{-i\omega t}C_{ee}(t)dt. \tag{B1}$$

The autocorrelation function

$$C_{ab}(t) \equiv \frac{1}{T}\int_0^T \delta\rho_a(t_1)\delta\rho_b(t_1 + t)dt_1, \tag{B2}$$

where $\delta\rho_a(t) = \rho_a(t) - \rho_a$ describes fluctuations of activity $\rho_a(t)$ of population a, $a = e,i$, around the averaged value ρ_a. $C_{ab}(t)$ is a measure of correlations between values of $\delta\rho_a(t_1)$ and $\delta\rho_b(t_1 + t)$ at two different instants separated by a lag t and averaged over an arbitrary large time window T (see, for example, in [80]).

In order to calculate the PSD, we assume that activity fluctuations are driven by weak white-noise forces $F_a(t)$ that mimic forces caused by finite-size effects

$$\langle F_a(t)F_b(t')\rangle = F_0^2\delta_{a,b}\delta(t - t'), \tag{B3}$$

where $F_0 \propto 1/\sqrt{N}$. In this case, one can use the linear response theory and find $\delta\rho_a(t) = \rho_a(t) - \rho$ from the linearized Eq. (6):

$$\frac{d\overrightarrow{\delta\rho}}{dt} = (1 - \rho)\overrightarrow{F} + \widehat{J}\overrightarrow{\delta\rho}, \tag{B4}$$

where ρ is a steady state solution of Eq. (8), $\overrightarrow{\delta\rho} = (\delta\rho_e,\delta\rho_i)$, and $\overrightarrow{F} = [F_e(t),F_i(t)]$. The Jacobian $\widehat{J}$ is given by Eq. (10).

Making the Fourier transformation

$$\delta\widetilde{\rho}_a(\omega) = \frac{1}{2\pi}\int_{-\infty}^{\infty} e^{-i\omega t}\delta\rho_a(t)d\omega, \tag{B5}$$

we find the linear response

$$\begin{aligned}\delta\widetilde{\rho}_e(\omega) &= \frac{(1-\rho)[(i\omega - J_{22})\widetilde{F}_e(\omega) + J_{12}\widetilde{F}_i(\omega)]}{(i\omega+\lambda_+)(i\omega+\lambda_-)},\\ \delta\widetilde{\rho}_i(\omega) &= \frac{(1-\rho)[J_{21}\widetilde{F}_e(\omega) + (i\omega - J_{11})\widetilde{F}_i(\omega)]}{(i\omega+\lambda_+)(i\omega+\lambda_-)}.\end{aligned} \tag{B6}$$

Substituting this result into Eq. (B2), we find the PSD for excitatory neurons

$$S(\omega) = \frac{F_0^2(1-\rho)^2}{2\pi}\frac{\left(J_{12}^2 + J_{22}^2 + \omega^2\right)}{(\lambda_+^2+\omega^2)(\lambda_-^2+\omega^2)}. \tag{B7}$$

The PSD of inhibitory neurons is obtained from this equation after replacements: $J_{12} \to J_{21}$ and $J_{22} \to J_{11}$.

1. PSD near the first-order phase transition

At first, let us consider the power spectral density (PSD) of activity fluctuations in the low activity state (the fixed point 1) in regions Ib and Ic in Fig. 2. In these regions, eigenvalues λ_+ and λ_- are real. When the noise intensity $\langle n\rangle$ tends to the critical point n_{c2} of the first-order phase transition, the eigenvalue λ_+ tends to zero according to Eq. (18) while the eigenvalue λ_- remains finite. Therefore, at small ω, Eq. (B7) takes a form

$$S(\omega) \approx \frac{F_0^2(1-\rho)^2(J_{12}^2+J_{22}^2)}{2\pi\lambda_-^2\gamma_r^2}\frac{1}{(\omega/\gamma_r)^2+1}. \tag{B8}$$

2. PSD near the Hopf bifurcation

Now, we consider the PSD of activity fluctuations in the high activity state (the fixed point 3) at $\langle n\rangle > n_{c3}$ (region IIb in Fig. 2). In this region, the eigenvalues $\lambda_\pm$ are complex. Their real and imaginary parts determine the relaxation rate γ_r and the frequency γ_i of damped oscillations, respectively [see Eqs. (12) and (13)]. In this case, Eq. (B7) can be written in a form

$$S(\omega) = \frac{F_0^2(1-\rho)^2}{2\pi\omega_0^4}\frac{\left(J_{12}^2 + J_{22}^2 + \omega_0^2x^2\right)}{[(x^2-1)^2 + 4\zeta^2x^2]}, \tag{B9}$$

where $x \equiv \omega/\omega_0$, $\omega_0 \equiv [\gamma_i^2+\gamma_r^2]^{1/2}$, and $\zeta \equiv \gamma_r/\omega_0$. ζ is the damping ratio of the damped oscillations.

In the case when the shot noise intensity $\langle n\rangle$ tends from above to the critical point n_{c3}, the relaxation rate γ_r tends to zero [see Eq. (25)]. If $\zeta \ll 1$, then the PSD has a sharp peak at the resonance frequency $\omega = \omega_r \equiv \omega_0(1-2\zeta^2)^{1/2}$. The peak maximum is

$$S_{\max} \equiv S(\omega_r) = \frac{F_0^2(1-\rho)^2}{2\pi\omega_0^4}\frac{[J_{12}^2 + J_{22}^2 + \omega_0^2(1-2\zeta^2)]}{4\zeta^2(1-\zeta^2)}. \tag{B10}$$

Near the resonance frequency $|\omega - \omega_r| \ll \omega_0$, $S(\omega)$ is described by a shape function $F(x,\zeta)$:

$$\frac{S(\omega)}{S_{\max}} \approx F(x,\zeta) \equiv \frac{4\zeta^2(1-\zeta^2)}{(1-x^2)^2 + 4\zeta^2x^2}. \tag{B11}$$

Substituting Eq. (B6) into (B2), we find that the autocorrelation function $C_{ee}(t)$ has a form

$$C_{ee}(t) = A_e e^{-\gamma_r t}\cos(\gamma_i t + \varphi_e). \tag{B12}$$

The amplitude A_e and the phase φ_e behave as $A_e \propto 1/\gamma_r$ and $\varphi_e \propto \gamma_r/\gamma_i$ at $\gamma_r \ll \gamma_i$. For inhibitory neurons, we obtain a similar behavior with A_i and the phase φ_i. There is a phase lag between maximums of excitatory and inhibitory activities,

$$\Delta\varphi = \varphi_e - \varphi_i \propto \gamma_r/\gamma_i, \tag{B13}$$

which is related with the time lag $\Delta t_l = \Delta\varphi/\gamma_i$.

APPENDIX C: OSCILLATIONS NEAR THE SUPERCRITICAL HOPF BIFURCATION: NONLINEAR ANALYSIS

In this Appendix, we study analytically oscillations and relaxation dynamics near the Hopf bifurcation in a shot noise intensity range $0 < |n_{c3} - \langle n\rangle| \ll n_{c3}$ (a range around the boundary between regions IIIa and IIb in Fig. 2). In this range, the oscillations have a small amplitude that allows us to use the Taylor expansion over $\delta\rho_a(t) = \rho_a(t) - \rho^{(3)}$ in Eqs. (6). Assuming $F_e = F_i = 0$ and taking into account terms up to the third order in $\delta\rho_a(t)$, we obtain two coupled nonlinear equations

$$\begin{aligned}\frac{d\delta\rho_a(t)}{\mu_a dt} &= -\delta\rho_a(t) + D^{(1,0)}\delta\rho_e(t) + D^{(0,1)}\delta\rho_i(t)\\ &+ \frac{1}{2}\left[D^{(2,0)}\delta\rho_e(t)^2 + 2D^{(1,1)}\delta\rho_e(t)\delta\rho_i(t)\right.\\ &\left. + D^{(0,2)}\delta\rho_i^2(t)\right]\\ &+ \frac{1}{6}\left[D^{(3,0)}\delta\rho_e^3(t) + 3D^{(2,1)}\delta\rho_e^2(t)\delta\rho_i(t)\right.\\ &\left. + 3D^{(1,2)}\delta\rho_e(t)\delta\rho_i^2(t) + D^{(0,3)}\delta\rho_i^3(t)\right],\end{aligned} \tag{C1}$$

where $a = e,i$ and

$$D^{(n,m)} \equiv \frac{\partial^{n+m}\Psi}{\partial\rho_e^n\partial\rho_i^m}. \tag{C2}$$

In Fig. 9(a), we compare results of numerical integration of the reduced equations (C1) with the exact equations (6). In the numerical integration, we studied relaxation of the system to a state with sustained oscillations [see Fig. 9(a)] from an initial point $\rho_e = \rho_i = \rho^{(3)}$. One sees that the frequency of the oscillations described by the reduced equations (C1) is very close to the frequency of oscillations from exact equations (6) though the amplitude of the sustained oscillations from Eqs. (C1) is a little bit larger. These results evidence that the reduced equations (C1) are a good approximation to the exact equations (6). A similar analysis based on a reduced equation was used in [14,15] to study analytically oscillations near the Hopf bifurcation in networks of integrate-and-fire neurons. Following, we use the reduced equations to study a critical behavior of the amplitude of sustained oscillations, a relaxation rate to the state with the oscillations, and the phase lag between activities of excitatory and inhibitory populations.

It is convenient to rewrite Eqs. (C1) in a vector form

$$\delta\dot{\vec{\rho}} = \hat{J}\delta\vec{\rho} + \hat{M}(\delta\rho_e,\delta\rho_i)\delta\vec{\rho}, \tag{C3}$$

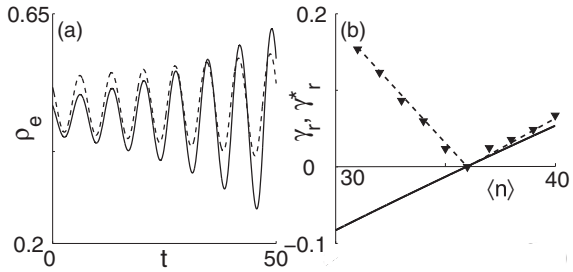

FIG. 9. (a) Relaxation of activity of excitatory neurons from an initial state (the fixed point 3) to a state with sustained network oscillations at $\langle n\rangle < n_{c3}$: (solid line) numerical integration of the approximate equations (C1); (dashed line) exact equations (6). (b) The parameter γ_r [Eq. (12)] versus $\langle n\rangle$ from a numerical solution of Eq. (8) at fixed point 3 (solid line). The relaxation rate γ_r^* is obtained from numerical integration of equations (6) (triangles). Parameters: $\langle n\rangle = 35$, $\alpha = 0.75$.

where

$$\delta\vec{\rho} = \begin{pmatrix} \delta\rho_e \\ \delta\rho_i \end{pmatrix}.$$

$\hat{J}$ is the Jacobian [Eq. (10)] and $\hat{M}(\delta\rho_e,\delta\rho_i)$ is a matrix which introduces nonlinear terms

$$\begin{aligned}
M_{11} &= \frac{1}{2}D^{(2,0)}\delta\rho_e + \frac{1}{6}D^{(3,0)}\delta\rho_e^2,\\
M_{12} &= \frac{1}{2}D^{(0,2)}\delta\rho_i + \frac{1}{6}D^{(0,3)}\delta\rho_i^2 + D^{(1,1)}\delta\rho_e\\
&\quad + \frac{1}{2}D^{(2,1)}\delta\rho_e^2 + \frac{1}{2}D^{(1,2)}\delta\rho_e\delta\rho_i,\\
M_{22} &= \frac{\alpha}{2}D^{(0,2)}\delta\rho_i + \frac{\alpha}{6}D^{(0,3)}\delta\rho_i^2,\\
M_{21} &= \frac{\alpha}{2}D^{(2,0)}\delta\rho_e + \frac{\alpha}{6}D^{(3,0)}\delta\rho_e^2 + \alpha D^{(1,1)}\delta\rho_i\\
&\quad + \frac{\alpha}{2}D^{(1,2)}\delta\rho_i^2 + \frac{\alpha}{2}D^{(2,1)}\delta\rho_e\delta\rho_i.
\end{aligned} \tag{C4}$$

The Jacobian $\hat{J}$ [Eq. (10)] can be represented in a form

$$\hat{J} = -\gamma_r\hat{I} + (\vec{a}\hat{\vec{\sigma}}), \tag{C5}$$

where $\hat{I}$ is the identity matrix. The parameter γ_r is determined by Eqs. (12) and (11) at the fixed point 3, i.e., $\rho_e = \rho_i = \rho^{(3)}$. In regions IIb and IIIa, Eq. (11) gives $\gamma_r = (J_{11} + J_{22})/2$. Furthermore, $\vec{a}$ is a complex vector $\vec{a}=(a_1,a_2,a_3)=\frac{1}{2}(J_{12}+J_{21},iJ_{12}-iJ_{21},J_{11}-J_{22})$ with the property $\vec{a}^2 = -\gamma_i^2$. We also use notations $\hat{\vec{\sigma}} = (\hat{\sigma}_1,\hat{\sigma}_2,\hat{\sigma}_3)$ where $\hat{\sigma}_1,\hat{\sigma}_2$, and $\hat{\sigma}_3$ are the Pauli matrices. Taking into account only linear terms in $\delta\rho_a$, the solution of Eq. (C3) can be written in a form

$$\delta\vec{\rho} = e^{-\gamma_r t+\vec{a}\hat{\vec{\sigma}}t}\vec{A} = e^{-\gamma_r t}\left[\cos(\gamma_i t) + \frac{\sin(\gamma_i t)}{\gamma_i}\vec{a}\hat{\vec{\sigma}}\right]\vec{A}, \tag{C6}$$

where the vector $\vec{A} = (A_e,A_i)$ is determined by an initial condition $\vec{\rho}(t=0) = \vec{\rho}_0$.

Dependence of the parameter γ_r on $\langle n\rangle$ near the critical point n_{c3} can be found by use of the Taylor expansion of $\mathrm{Re}\lambda_+(\rho^{(3)})$ in Eq. (12) over $\delta\rho = \rho^{(3)} - \rho^{(3)}(n_{c3})$:

$$\gamma_r(\rho^{(3)}) = -\mathrm{Re}\lambda_+[\rho^{(3)}(n_{c3})] - \frac{d\,\mathrm{Re}\lambda_+}{d\rho}\delta\rho + \ldots. \tag{C7}$$

Taking into account the critical slowing down, Eq. (15), and Eq. (A5) we obtain

$$\gamma_r \approx \Gamma(\langle n\rangle - n_{c3}), \tag{C8}$$

where the coefficient Γ is positive according to our numerical estimations. At $\langle n\rangle > n_{c3}$, γ_r is positive and neuronal activity weakly perturbed from the stable fixed point 3 [$\rho_e = \rho_i = \rho(3)$] relaxes exponentially to the steady state with the relaxation rate γ_r [see Eq. (C6)]. At $\langle n\rangle < n_{c3}$, γ_r is negative and describes the process of runaway from the fixed point 3 [see Figs. 5(b) and 9(b)]. In order to find a correct solution of Eq. (C3) and the relaxation rate in the state with sustained network oscillations, we must take into account nonlinear terms. We look for a solution in the following form:

$$\delta\vec{\rho} = e^{\vec{a}\hat{\sigma}t}\vec{A}(t). \tag{C9}$$

Then, Eq. (C3) takes a form

$$\dot{\vec{A}} = -\gamma_r\vec{A} + e^{-\vec{a}\hat{\sigma}t}\hat{M}(\delta\rho_e,\delta\rho_i)e^{\vec{a}\hat{\sigma}t}\vec{A}. \tag{C10}$$

In the leading order in $\varepsilon = n_{c3} - \langle n\rangle$, in the limit $t\to\infty$, the oscillation amplitude $\vec{A}(t)$ tends to a stationary value that can be found by use of the averaging theory [9]. We integrate Eq. (C10) over the period $T = 2\pi/\gamma_i$ of oscillations,

$$0 = \int_0^T\{-\gamma_r\vec{A} + e^{-\vec{a}\hat{\sigma}t}\hat{M}[\delta\rho_e(t),\delta\rho_i(t)]e^{\vec{a}\hat{\sigma}t}\vec{A}\}dt, \tag{C11}$$

and obtain two coupled equations for A_e and A_i:

$$\begin{aligned}
0 &= -\gamma_r A_e + a_1^{(e)}A_e^3 + a_2^{(e)}A_e^2A_i + a_3^{(e)}A_eA_i^2 + a_4^{(e)}A_i^3,\\
0 &= -\gamma_r A_i + a_1^{(i)}A_i^3 + a_2^{(i)}A_i^2A_e + a_3^{(i)}A_iA_e^2 + a_4^{(i)}A_e^3,
\end{aligned} \tag{C12}$$

where $a_n^{(a)}$ are coefficients. A simple analysis of these equations shows that, at $|\gamma_r| \ll 1$, a solution for the complex amplitudes A_e and A_i has a form

$$\vec{A} = \sqrt{|\gamma_r|}\vec{B} \propto \sqrt{n_{c3} - \langle n\rangle}\vec{B}, \tag{C13}$$

where $\vec{B} = (e^{i\varphi_e}b_e,e^{i\varphi_i}b_i)$ is a complex vector and $\Delta\varphi \equiv \varphi_e - \varphi_i$ is a phase lag between excitatory and inhibitory activities. The square root dependence in Eq. (C13) agrees with the numerical solution of Eqs. (6) for the supercritical Hopf bifurcation [see Fig. 5(c)]. This dependence is a general property of the supercritical Hopf bifurcation.

APPENDIX D: RELAXATION RATE AND PHASE LAG

Equation (C10) also allows us to find the relaxation rate of perturbed neuronal activity in the region IIIa with sustained network oscillations. We denote the relaxation rate as γ_r^* in order to distinguish it from the parameter γ_r. We look for a solution of Eq. (C10) in a form

$$\vec{A}(t) = \vec{A} + e^{-\gamma_r^* t}\delta\vec{A}, \tag{D1}$$

where $\delta\vec{A}$ is a small perturbation and $\gamma_r^* \ll \gamma_i$ is assumed. A linear perturbation analysis with respect to $\delta\vec{A}$ gives

$$\gamma_r^* \approx G(n_{c3} - \langle n \rangle), \tag{D2}$$

where G is a positive coefficient. γ_r^* tends to zero when $\langle n \rangle \to n_{c3}$. Results of our numerical calculations displayed in Fig. 9(b) agree with this result. In numerical integration of Eqs. (6), we chose the fixed point 3 as an initial condition, i.e., $\rho_e = \rho_i = \rho^{(3)}$ at the initial time $t = 0$. Since the point 3 is unstable, at first the amplitude of network oscillations exponentially increases in time with the rate $-\gamma_r$ [see Fig. 9(a)]. At large t, the amplitude tends exponentially (with the relaxation rate γ_r^*) to a steady value.

Solving Eq. (C12), we find the phases φ_e and φ_i. The lag $\Delta\varphi = \varphi_e - \varphi_i$ is proportional to $|\gamma_r| \propto n_{c3} - \langle n \rangle$, i.e.,

$$\Delta\varphi \approx \psi^*(n_{c3} - \langle n \rangle), \tag{D3}$$

where ψ^* is a positive coefficient. At $\langle n \rangle \geqslant n_{c3}$, i.e., in the state with damped oscillations, the phase lag $\Delta\varphi$ is determined by Eqs. (B13) and (C8) that give

$$\Delta\varphi \approx \psi(\langle n \rangle - n_{c3}), \tag{D4}$$

where the coefficient ψ differs from ψ^*. Thus, the phase lag $\Delta\varphi$ is zero at the critical point and increases with increasing distance $|\langle n \rangle - n_{c3}|$ from the critical point.

[1] J. A. S. Kelso, *Dynamic Patterns: The Self-Organization of Brain and Behavior* (The MIT Press, Cambridge, 1995).
[2] D. R. Chialvo, Nat. Phys. **2**, 301 (2006); **6**, 744 (2010).
[3] G. Buzsáki, *Rhythms of the Brain* (Oxford University Press, Oxford, 2006).
[4] J. A. Kelso, Am. J. Physiol.: Regul., Integr. Comp. Physiol. **246**, R1000 (1984).
[5] H. Haken, J. A. S. Kelso, and H. Bunz, Biol. Cybern. **51**, 347 (1985).
[6] J. A. Kelso, J. Scholz, and G. Schöner, Phys. Lett. A **118**, 279 (1986).
[7] D. Steyn-Ross and M. Steyn-Ross, *Modeling Phase Transitions in the Brain*. Springer Series in Computational Neuroscience, Vol. 4 (Springer, New York, 2010).
[8] I. Breskin, J. Soriano, E. Moses, and T. Tlusty, Phys. Rev. Lett. **97**, 188102 (2006).
[9] S. H. Strogatz, *Nonlinear Dynamics And Chaos: With Applications To Physics, Biology, Chemistry, And Engineering* (Perseus Books Group, New York, 1994).
[10] Yuri A. Kuznetsov, *Elements of Applied Bifurcation Theory* (Springer, New York, 1998).
[11] J. Rinzel and G. B. Ermentrout, in *Methods in Neuronal Modeling*, edited by C. Koch and I. Segev (The MIT Press, Cambridge, 1989), p. 251.
[12] E. M. Izhikevich, Int. J. Bif. and Chaos **10**, 1171 (2000).
[13] D. J. Amit and N. Brunel, Cereb. Cortex **7**, 237 (1997).
[14] N. Brunel and V. Hakim, Neural Comput. **11**, 1621 (1999).
[15] N. Brunel, J. Comput. Neurosci. **8**, 183 (2000).
[16] S. Ostojic, N. Brunel, and V. Hakim, J. Comput. Neurosci. **26**, 369 (2009).
[17] E. Ledoux and N. Brunel, Front. Comput. Neurosci. **5**, 25 (2011).
[18] B. Lindner, B. Doiron, and A. Longtin, Phys. Rev. E **72**, 061919 (2005).
[19] N. Brunel and V. Hakim, Chaos **18**, 015113 (2008).
[20] D. Millman, S. Mihalas, A. Kirkwood, and E. Niebur, Nat. Phys. **6**, 801 (2010).
[21] M. Benayoun, J. D. Cowan, W. van Drongelen, and E. Wallace, PLoS Comput. Biol. **6**, e1000846 (2010).
[22] E. Wallace, M. Benayoun, W. van Drongelen, and J. D. Cowan, PLoS ONE **6**, e14804 (2011).
[23] H. E. Stanley, *Introduction to Phase Transitions and Critical Phenomena* (Oxford University Press, London, 1987).
[24] J. M. Beggs and D. Plenz, J. Neurosci. **23**, 11167 (2003).
[25] D. Plenz and T. C. Thiagarajan, Trends Neurosci. **30**, 101 (2007).
[26] M. Steriade and D. Contreras, J. Neurosci. **15**, 623 (1995).
[27] I. Timofeev and M. Steriade, Neurosci. **123**, 299 (2004).
[28] G. Buzsáki, Brain Res. **398**, 242 (1986).
[29] C. S. Rex, L. L. Colgin, Y. Jia, M. Casale, T. K. Yanagihara, M. Debenedetti, C. M. Gall, E. A. Kramar, and G. Lynch, PLoS One **4**, e7761 (2009).
[30] D. Contreras, A. Destexhe, T. J. Sejnowski, and M. Steriade, Science **274**, 771 (1996).
[31] M. Scheffer, J. Bascompte, W. A. Brock, V. Brovkin, S. R. Carpenter, V. Dakos, H. Held, E. H. van Nes, M. Rietkerk, and G. Sugihara, Nature (London) **461**, 53 (2009).
[32] R. J. Baxter, *Exactly Solved Models in Statistical Mechanics* (Academic, San Diego, 1982).
[33] C. Morris and H. Lecar, Biophys. J. **35**, 193 (1981).
[34] R. Albert and A. L. Barabasi, Rev. Mod. Phys. **74**, 47 (2002).
[35] S. N. Dorogovtsev and J. F. F. Mendes, Adv. Phys. **51**, 1079 (2002).
[36] M. E. J. Newman, SIAM Review **45**, 167 (2003).
[37] O. Sporns, D. R. Chialvo, M. Kaiser, and C. C. Hilgetag, Trends Cogn. Sci. **8**, 418 (2004).
[38] J. A. White, J. T. Rubinstein, and A. R. Kay, Trends Neurosci. **23**, 131 (2000).
[39] B. Lindner, J. Garcia-Ojalvo, A. Neiman, and L. Schimansky-Geier, Phys. Rep. **392**, 321 (2004).
[40] A. A. Faisal, L. P. J. Selen, and D. M. Wolpert, Nat. Rev. **9**, 292 (2008).
[41] G. B. Ermentrout, R. F. Galan, and N. N. Urban, Trends Neurosci. **31**, 428 (2008).
[42] A. V. Goltsev, F. V. de Abreu, S. N. Dorogovtsev, and J. F. F. Mendes, Phys. Rev. E **81**, 061921 (2010).
[43] D. Holstein, A. V. Goltsev, and J. F. F. Mendes, Phys. Rev. E **87**, 032717 (2013).
[44] J.-P. Eckmann, O. Feinerman, L. Gruendlinger, E. Moses, J. Soriano, and T. Tlusty, Phys. Rep. **449**, 54 (2007).
[45] J. Soriano, M. Rodríguez Martínez, T. Tlusty, and E. Moses, Proc. Natl. Acad. Sci. USA **105**, 13758 (2008).
[46] P. Heil, Curr. Opin. Neurobiol. **14**, 461 (2004).
[47] H. A. Swadlow, Cerebral Cortex **13**, 25 (2003).

[48] S. Fujisawa, N. Matsuki, and Y. Ikegaya, J. Physiol. (Oxford, UK) **561**, 123 (2004).
[49] M. L. Molineux, F. R. Fernandez, W. H. Mehaffey, and R. W. Turner, J. Neurosci. **25**, 10863 (2005).
[50] S. N. Dorogovtsev, A. V. Goltsev, and J. F. F. Mendes, Rev. Mod. Phys. **80**, 1275 (2008).
[51] H. R. Wilson and J. D. Cowan, Biophys. J. **12**, 1 (1972); Kybernetik **13**, 55 (1973).
[52] M. A. Lopes, A. V. Goltsev., K. E. Lee, and J. F. F. Mendes, in *Physics, Computation, and the Mind: Advances and Challenges at Interfaces*, edited by P. L. Garrido, J. Marro, J. J. Torres, and J. M. Cortes, AIP Conference Proceedings, 1510 (Melville, New York, 2013), pp. 202–206,
[53] K.-E. Lee, A. V. Goltsev, M. A. Lopes, and J. F. F. Mendes, in *Physics, Computation, and the Mind: Advances and Challenges at Interfaces*, edited by P. L. Garrido, J. Marro, J. J. Torres, and J. M. Cortes, AIP Conference Proceedings, 1510 (Melville, New York, 2013), pp. 195–201.
[54] J. G. Orlandi, J. Soriano, E. Alvarez-Lacalle, S. Teller, and J. Casademunt, Nat. Phys. (to be published).
[55] N. Friedman, S. Ito, B. A. W. Brinkman, M. Shimono, R. E. Lee DeVille, K. A. Dahmen, J. M. Beggs, and T. C. Butler, Phys. Rev. Lett. **108**, 208102 (2012).
[56] A. Clauset, C. R. Shalizi, and M. E. J. Newman, SIAM Rev. **51**, 661 (2009).
[57] We used the software presented in http://tuvalu.santafe.edu/∼aaronc/powerlaws/. The tail of the avalanche size distribution $P(s)$ follows a power law with the exponent $z = 1.50$ for values greater than $s_{\min} = 1767$ with the log-likelihood $L = -231.4$, the Kolmogorov-Smirnov statistic $D = 0.069$, $p = 0.88$, and with the finite-size correction. This value of $s_{\min}$ minimizes D.
[58] J. P. Sethna, K. Dahmen, S. Kartha, J. A. Krumhansl, B. W. Roberts, and J. D. Shore, Phys. Rev. Lett. **70**, 3347 (1993).
[59] J. P. Sethna, K. Dahmen, and C. R. Myers, Nature (London) **410**, 242 (2001).
[60] A. V. Goltsev, S. N. Dorogovtsev, and J. F. F. Mendes, Phys. Rev. E **73**, 056101 (2006).
[61] S. N. Dorogovtsev, A. V. Goltsev, and J. F. F. Mendes, Phys. Rev. Lett. **96**, 040601 (2006).
[62] G. J. Baxter, S. N. Dorogovtsev, A. V. Goltsev, and J. F. F. Mendes, Phys. Rev. Lett. **109**, 248701 (2012).
[63] J. Soriano and E. Moses (private communication).
[64] E. M. Izhikevich and G. M. Edelman, Proc. Natl. Acad. Sci. USA **105**, 3593 (2008).
[65] D. Stauffer and A. Aharony, *Introduction to Percolation Theory* (Taylor and Francis, London, 2003).
[66] K. Binder, Ferroelectrics **73**, 43 (1987).
[67] C. Bédard, H. Kröger, and A. Destexhe, Phys. Rev. Lett. **97**, 118102 (2006).
[68] P. Bak, *How Nature Works* (Oxford University Press, Oxford, UK, 1997).
[69] Hu Gang, T. Ditzinger, C. Z. Ning, and H. Haken, Phys. Rev. Lett. **71**, 807 (1993).
[70] W.-J. Rappel and S. H. Strogatz, Phys. Rev. E **50**, 3249 (1994).
[71] K. Wiesenfeld, D. Pierson, E. Pantazelou, C. Dames, and F. Moss, Phys. Rev. Lett. **72**, 2125 (1994).
[72] A. Longtin, Phys. Rev. E **55**, 868 (1997).
[73] W. C. Stacey and D. M. Durand, J. Neurophysiol. **83**, 1394 (2000); **86**, 1104 (2001).
[74] P. C. Matthews and S. H. Strogatz, Phys. Rev. Lett. **65**, 1701 (1990).
[75] K. Krischer, M. Eiswirth, and G. Ertl, J. Chem. Phys. **96**, 9161 (1992).
[76] A. Babloyantz and A. Destexhe, Proc. Natl. Acad. Sci. USA **83**, 3513 (1986).
[77] R. Hari and R. Salmelin, Trends Neurosci. **20**, 44 (1997).
[78] L. Lehtel, R. Salmelin, and R. Hari, Neurosci. Lett. **222**, 111 (1997).
[79] L. F. Abbott, in *23 Problems in Systems Neuroscience (Computational Neuroscience Series)*, edited by J. L. van Hemmen and T. J. Sejnowski (Oxford University Press, Oxford, UK, 2006), p. 423.
[80] C. W. Gardiner, *Handbook of Stochastic methods: For Physics, Chemistry and the Natural Sciences* (Springer, Berlin, 2002).